

Universality in the three-dimensional random-field Ising model

Nikolaos G. Fytas^{1,2} and Víctor Martín-Mayor^{1,3}

¹*Departamento de Física Teórica I, Universidad Complutense, E-28040 Madrid, Spain.*

²*Applied Mathematics Research Centre, Coventry University, Coventry, CV1 5FB, United Kingdom.*

³*Instituto de Biocomputación and Física de Sistemas Complejos (BIFI), E-50009 Zaragoza, Spain.*

We solve a long-standing puzzle in Statistical Mechanics of disordered systems. By performing a high-statistics simulation of the $D = 3$ random-field Ising model at zero temperature for different shapes of the random-field distribution, we show that the model is ruled by a single universality class. We compute the complete set of critical exponents for this class, including the correction-to-scaling exponent, and we show, to high numerical accuracy, that scaling is described by two independent exponents. Discrepancies with previous works are explained in terms of strong scaling corrections.

PACS numbers: 75.10.Nr, 02.60.Pn, 75.50.Lk

The random-field Ising model (RFIM), is one of the simplest and most investigated models for collective behavior in the presence of quenched disorder [1]. In spite of its simplicity, many problems in Condensed Matter Physics can be studied through the RFIM: diluted antiferromagnets in a field [2], colloid-polymer mixtures [4, 5], colossal magnetoresistance oxides [6, 7] (more generally, phase-coexistence in the presence of quenched disorder [8–10]), non-equilibrium phenomena such as the Barkhausen noise in magnetic hysteresis [11, 12] or the design of switchable magnetic domains [13], etc.

On the theoretical side, a scaling picture is available [14–17]. The paramagnetic-ferromagnetic phase transition is ruled by a fixed-point [in the Renormalization-Group (RG) sense] at temperature $T = 0$ [1]. The spatial dimension D is replaced by $D - \theta$, in hyperscaling relations ($\theta \approx D/2$). Nevertheless, many expect only two independent exponents [1, 18, 19], as in standard phase transitions (see e.g. [20]).

Unfortunately, establishing the scaling picture is far from trivial. Perturbation theory predicts that, in $D = 3$, the ferromagnetic phase disappears upon applying the tiniest random field [21]. Even if the statement holds at all orders in perturbation theory [22], the ferromagnetic phase is stable in $D = 3$ [23]. Nonperturbative phenomena are obviously at play [24, 25]. Indeed, it has been suggested that the scaling picture breaks down because of spontaneous supersymmetry breaking, implying that more than two critical exponents are needed to describe the phase transition [26].

On the experimental side, a particularly well researched realization of the RFIM is the diluted antiferromagnet in an applied magnetic field [2]. Yet, there are inconsistencies in the determination of critical exponents. In neutron scattering, different parameterizations of the scattering line-shape yield mutually incompatible estimates of the thermal critical exponent, namely $\nu = 0.87(7)$ [27] and $\nu = 1.20(5)$ [28]. Moreover, the anomalous dimension $\eta = 0.16(6)$ [27] violates hyperscaling bounds (at least if one believes experimental claims of a divergent specific heat [29, 30]). Clearly, a reliable parametrization of the line-shape would be welcome. This program has been carried out for simpler, better un-

derstood problems [31]. Unfortunately, we do not have such a strong command over the RFIM universality class.

The RFIM has been also investigated by means of numerical simulations. However, typical Monte Carlo schemes get trapped into local minima with escape time exponential in ξ^θ (ξ is the correlation length). Although sophisticated improvements have appeared [32–34], these simulations produced low-accuracy data because they were limited to linear sizes $L \leq 32$. Larger sizes can be achieved at $T = 0$, through the well-known mapping of the ground state to the maximum-flow optimization problem [35–45]. Yet, $T = 0$ simulations lack many tools, standard at $T > 0$. In fact, the numerical data at $T = 0$ and their finite-size scaling analysis mostly resulted in strong universality violations [34, 37–40].

Here we show that the $D = 3$ RFIM is ruled by a single universality class, by considering explicitly four different models that belong to it. To this end, we perform high-statistics $T = 0$ simulations of the model and we introduce a fluctuation-dissipation formalism in order to compute connected and disconnected correlation functions. Another asset of our implementation is the use of phenomenological renormalization [46, 47], that allows us to extract effective size-dependent critical exponents, whose size evolution can be closely followed. Although the four models differ in their prediction for finite sizes, we show that, after a proper consideration of the scaling corrections, we can extrapolate to infinite-limit size, finding consistent results for all of them.

Our $S_x = \pm 1$ spins are on a cubic lattice with size L and periodic boundary conditions. The Hamiltonian is

$$\mathcal{H} = -J \sum_{\langle x,y \rangle} S_x S_y - \sum_x h_x S_x. \quad (1)$$

$J = 1$ is the nearest-neighbors' ferromagnetic interaction. Independent quenched random fields h_x are extracted from one of the following double Gaussian (dG) or Poissonian (P) distributions (with parameters h_R, σ):

$$\text{dG}^{(\sigma)}(h_x; h_R) = \frac{1}{\sqrt{8\pi\sigma^2}} \left[e^{-\frac{(h_x - h_R)^2}{2\sigma^2}} + e^{-\frac{(h_x + h_R)^2}{2\sigma^2}} \right], \quad (2)$$

$$\text{P}(h_x; \sigma) = \frac{1}{2|\sigma|} e^{-|h_x|/\sigma}. \quad (3)$$

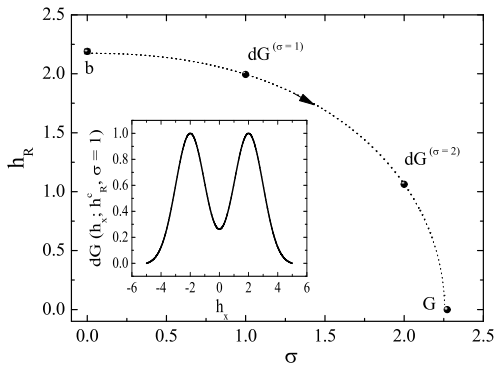


FIG. 1: Phase diagram of the double Gaussian RFIM, Eq. (2), at $T = 0$. The dotted critical line (a simple guide to the eye) separates the paramagnetic phase (low σ , h_R) from the ordered phase (large σ , h_R). Transition points are computed here (data from Table IV in the Appendix), but for the limit $\sigma = 0$ which corresponds to binary random fields [40]. The arrow along the critical line indicates the RG flow. **Inset:** bimodal shape of the critical double Gaussian distribution (2) with $\sigma = 1$.

The limiting cases $\sigma = 0$ and $h_R = 0$ of Eq. (2) correspond to the well-known bimodal (b) and Gaussian (G) distributions, respectively. In the P and G cases the strength of the random fields is parameterized by σ , while in the dG case we shall take $\sigma = 1$ and 2, and vary h_R . The phase diagram for the double Gaussian distribution is sketched in Fig. 1. Note the bimodal shape of Eq. (2) for $\sigma = 1$, with peaks near $\pm h_R$.

An instance of the random fields $\{h_x\}$ is named a sample. The only relevant spin configurations at $T = 0$ are ground states, which are non-degenerate for continuous random-field distributions [48]. Thermal mean values are denoted as $\langle \dots \rangle$. The subsequent average over samples is indicated by an over-line (e.g., for the magnetization density $m = \sum_x s_x / L^D$ we consider both $\langle m \rangle$ and $\overline{\langle m \rangle}$).

We considered four disorder distributions: P, G and dG with $\sigma = 1, 2$. We obtained the ground-states using the push-relabel algorithm [49]. We implemented in C the algorithm in [42, 43], with periodic global updates. Our lattices sizes were $L = 12, 16, 24, 32, 48, 64, 96, 128$ and 192 [$16 \leq L \leq 128$ for $dG^{(\sigma=1)}$ and $12 \leq L \leq 128$ for $dG^{(\sigma=2)}$]. For each L , we averaged over 10^7 samples [5×10^7 samples for $dG^{(\sigma=1)}$]. Previous studies were limited to $\sim 10^4$ samples [41, 42].

We have generalized the fluctuation-dissipation formalism of [50] to compute connected $G_{xy} = \partial[\langle S_x \rangle] / \partial h_y$ and disconnected $G_{xy}^{(\text{dis})} = \overline{\langle S_x S_y \rangle}$ correlation functions. We compute from them the second-moment connected (ξ) and disconnected ($\xi^{(\text{dis})}$) correlation lengths [20, 51].

We have also extended reweighting methods from percolation studies [52, 53]. From a single simulation, we extrapolate the mean value of observables to nearby parameters of the disorder distribution (we varied σ for the

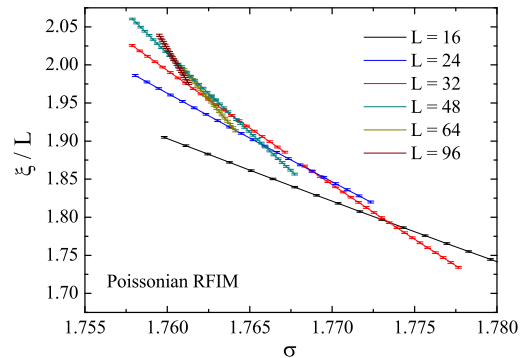


FIG. 2: (Color online) For several system sizes, we show ξ/L vs. the strength of the Poissonian random field σ [see Eq. (3)] (ξ : correlation length from the connected correlator, L : system size). Lines join data obtained from reweighting extrapolation, Eq. (4) (discontinuous lines of the same color come from independent simulations). In the large- L limit, ξ/L is L -independent at the critical point σ^c . In the quotients method, we consider the ξ/L curves for pair of lattices $(L, 2L)$ and seek the σ where they *cross*. This crossing is employed for computing effective, L -dependent critical exponents with Eq. (5).

G and P distributions, see Fig. 2, and h_R for the dG case). Computing derivatives with respect to σ or h_R is straightforward. Consider, for instance, the P case (see [54] for other distributions). Let $\mathcal{D} = \sum_x (|h_x| - \sigma) / \sigma^2$. The connected correlation function is $G_{xy} = \overline{h_y \langle S_x \rangle} / (\overline{|h_y| \sigma})$, while the σ -derivative and the reweighting-extrapolation to $\sigma + \delta\sigma$ of a generic observable O are

$$\begin{aligned} D_\sigma \overline{\langle O \rangle}_\sigma &= \overline{\langle OD \rangle}_\sigma, \quad \overline{\langle O \rangle}_{\sigma+\delta\sigma} = \overline{\langle OR \rangle}_\sigma \quad \text{with} \quad (4) \\ \mathcal{R} &= \exp \left[\mathcal{D} \frac{\sigma \delta\sigma}{\sigma + \delta\sigma} + L^D \left(\log \frac{\sigma}{\sigma + \delta\sigma} + \frac{\sigma + \delta\sigma}{\sigma} \right) \right]. \end{aligned}$$

To extract the value of critical points, critical exponents, and dimensionless quantities, we employ the quotients method [20, 46, 47]. We compare observables computed in pair of lattices $(L, 2L)$. We start imposing scale-invariance by seeking the L -dependent critical point: the value of σ (h_R for the dG), such that $\xi_{2L} / \xi_L = 2$ (i.e. the *crossing* point for ξ_L / L , see Fig 2). Now, for dimensionful quantities O , scaling in the thermodynamic limit as $\xi^{x_O/\nu}$, we consider the quotient $Q_O = O_{2L} / O_L$ at the crossing. For dimensionless magnitudes g , we focus on g_{2L} . In either case, one has:

$$Q_O^{\text{cross}} = 2^{x_O/\nu} + \mathcal{O}(L^{-\omega}), \quad g_{(2L)}^{\text{cross}} = g^* + \mathcal{O}(L^{-\omega}), \quad (5)$$

where x_O/ν , g^* and the scaling-corrections exponent ω are universal. Examples of dimensionless quantities are ξ/L , $\xi^{(\text{dis})}/L$ and $U_4 = \overline{\langle m^4 \rangle} / \overline{\langle m^2 \rangle}^2$. Instances of dimensionful quantities are the derivatives of ξ , $\xi^{(\text{dis})}$ ($x_\xi = 1 + \nu$), the connected and disconnected susceptibilities χ and $\chi^{(\text{dis})}$ [$x_\chi = \nu(2 - \eta)$, $x_{\chi^{(\text{dis})}} = \nu(4 - \bar{\eta})$], and the ratio $U_{22} = \chi^{(\text{dis})} / \chi^2$ [$x_{U_{22}} = \nu(2\eta - \bar{\eta})$].

TABLE I: For our four field distributions, size-dependent critical exponents of the $D = 3$ RFIM as computed from the quotients method.

Distr.	(L_1, L_2)	ν	η	$2\eta - \bar{\eta}$
G	(16, 32)	1.48(3)	0.5168(6)	0.0038(11)
	(24, 48)	1.45(3)	0.5155(5)	0.0022(11)
	(32, 64)	1.36(4)	0.5150(5)	0.0019(10)
	(48, 96)	1.43(6)	0.5154(5)	0.0033(9)
	(64, 128)	1.38(9)	0.5142(5)	0.0014(10)
dG $^{(\sigma=1)}$	(16, 32)	3.04(14)	0.5035(7)	0.0016(15)
	(24, 48)	2.26(9)	0.5083(7)	0.0034(14)
	(32, 64)	1.87(8)	0.5093(7)	0.0010(13)
	(48, 96)	1.56(9)	0.5121(7)	0.0026(14)
	(64, 128)	1.67(12)	0.5125(8)	0.0015(17)
dG $^{(\sigma=2)}$	(16, 32)	1.48(5)	0.5154(6)	0.0020(12)
	(24, 48)	1.50(6)	0.5151(7)	0.0020(13)
	(32, 64)	1.41(8)	0.5142(7)	0.0004(13)
	(48, 96)	1.36(10)	0.5148(7)	0.0024(14)
	(64, 128)	1.31(11)	0.5154(6)	0.0041(13)
P	(16, 32)	1.20(2)	0.5183(9)	-0.0006(19)
	(24, 48)	1.26(3)	0.5168(8)	0.0011(17)
	(32, 64)	1.30(4)	0.5153(8)	0.0005(17)
	(48, 96)	1.37(7)	0.5143(9)	0.0004(18)
	(64, 128)	1.33(7)	0.5148(8)	0.0024(16)
(96, 192)	1.43(13)	0.5146(8)	0.0026(17)	

The application of Eq. (5) to our four random-field distributions is summarized in Table I and Figs. 3 and 4 (the numerical values are listed in Table IV in the Appendix). We start inspecting ξ/L in Fig. 3. At fixed L , the dependence on the distribution is substantial. However, the strong size evolution suggests a common $L \rightarrow \infty$ limit. The behavior of the critical exponents, $\xi^{(\text{dis})}/L$ and U_4 is similar.

In order to extrapolate to $L \rightarrow \infty$, one fits the data of Table I to polynomials in $L^{-\omega}$. Although the procedure is standard [53], it has not been attempted before for the RFIM. Our extrapolations are documented in Fig. 4 and Table II. Several comments are in order:

- For dimensionless quantities we needed a third-order polynomial in $L^{-\omega}$ (only a subclass of the sub-leading corrections-to-scaling [20]). Leading-order corrections sufficed for critical exponents.
- We are not aware of any other computation of ω , ξ/L , $\xi^{(\text{dis})}/L$, and U_4 . All of them are universal.
- The full critical line belongs to a single universality class (justifying *a posteriori* the RG flow in Fig. 1). The fixed point at $\sigma = 0$ (bimodal RFIM) [37–40] has no basin of attraction.

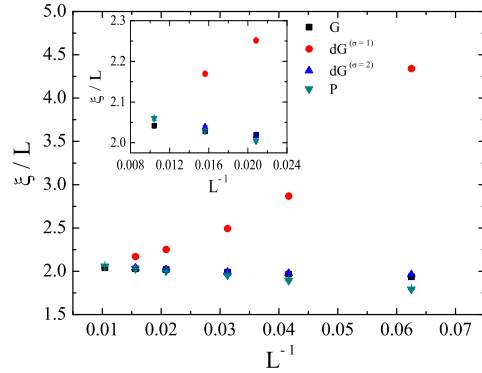


FIG. 3: (Color online) Inspection of the size-dependence of universal quantities. We show the universal ratio ξ/L versus $1/L$, as computed at the corresponding crossing points (see Fig 2) for the four disorder distributions considered in this work. The inset is an enlargement for $L \geq 48$.

TABLE II: Extrapolations to $L = \infty$ for the critical ξ/L , $\xi^{(\text{dis})}/L$, U_4 and the exponents of the $D = 3$ RFIM, (finite- L data from Table IV in the Appendix). We perform joint fits for sizes $L \geq L_{\text{min}}$ to polynomials in $L^{-\omega}$, imposing common extrapolations for all four random-field distributions. The χ^2 figure of merit was computed with the full covariance matrix (dof: number of degrees of freedom in the fit). For the exponent ν , we considered derivatives of both ξ and $\xi^{(\text{dis})}$. The error induced by the uncertainty in ω is given as a second error estimate. The extrapolation of the critical points slightly differs [56].

Extrapolation	χ^2/dof	L_{min}	order in $L^{-\omega}$
$(\xi/L) _{L=\infty} = 2.08(13)$			
$(\xi^{(\text{dis})}/L) _{L=\infty} = 8.4(8)$	18.8/14	24	third
$U_4 _{L=\infty} = 1.0011(18)$			
$\omega = 0.52(11)$			
$\nu _{L=\infty} = 1.38(10)(0.03)$	12.5/10	32	first
$\eta _{L=\infty} = 0.5153(9)(2)$	10.0/9	32	first
$(2\eta - \bar{\eta}) _{L=\infty} = 0$ (fixed)	18.3/18	16	first
$(2\eta - \bar{\eta}) _{L=\infty} = 0.0026(9)(1)$	10.5/17	16	first
$\sigma^c[\text{G}] = 2.27205(18)(4)$	3.1/3	16	second
$h_R^c[\text{dG}^{(\sigma=1)}] = 1.9955(6)(24)$	2.5/1	24	second
$h_R^c[\text{dG}^{(\sigma=2)}] = 1.0631(7)(10)$	0.7/2	16	second
$\sigma^c[\text{P}] = 1.7583(2)(2)$	3.0/3	16	second

- The two-exponent scaling scenario [1] ($2\eta = \bar{\eta}$) is supported by our data. Violations are at most ~ 0.002 , much smaller than predicted in [26].
- Our ν estimation is similar to modern computations [41, 43–45]. For the anomalous dimension, we note $\eta = 0.50(3)$ [41]. With some caution, we quote as well [57]. Our errors for ν are larger than for η or $\bar{\eta}$ because we compute derivatives as connected

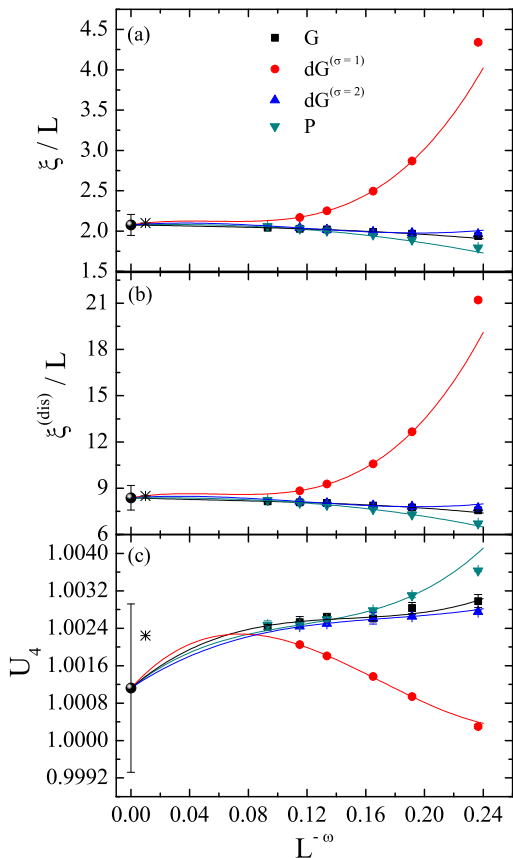


FIG. 4: (Color online) Computation of the corrections-to-scaling exponent ω , see Eq. (5), by means of a joint fit for ξ/L (a), $\xi^{(\text{dis})}/L$ (b), and $U_4 = \overline{\langle m^4 \rangle} / \overline{\langle m^2 \rangle}^2$ (c), see Table II and [55]. Black circles depicted at $L^{-\omega} = 0$ are our extrapolations to $L = \infty$. Stars denote extrapolations obtained using only the diagonal terms of the covariance matrix.

correlations, Eq. (4).

- The two-exponent scenario implies for the hyperscaling violation exponent $\theta = 2 - \eta = 1.4847(11)$ (recall $\theta = 1.469(20)$ [32] or $1.49(3)$ [42]).
- For the Gaussian RFIM, our critical point compares favorably to the value $2.270(4)$ of Ref. [42].

Where do we stand, at this point? Clearly, our confirmation of Universality provides motivation to undertake an ambitious field-theoretic study of the RFIM. The task is difficult, though. The direct approach of Refs. [21, 22] fails because the supersymmetry is spon-

taneously broken as soon as $\theta = 2$. The phenomenological two-exponent scaling picture [18, 19] seems highly successful, but it has not yet been derived from field theory. However, it does suggest a systematic way of computing critical exponents: study the ferromagnetic Ising model in the absence of disorder, but with a non-integer spatial dimension $d' = D - \theta$ [19] ($d' \approx 1.5153(11)$ according to our results for $D = 3$). The computation has been attempted within the ϵ -expansion, where $\epsilon = 4 - d'$. The results up to order ϵ^5 are encouraging, but not very accurate [58]. On the other hand, a first-principles approach, the functional Renormalization Group (fRG) [59], does explain the spontaneous breaking of the supersymmetry [26]. Yet, the fRG prediction for the critical exponents is rather crude. Furthermore, the smallness of $2\eta - \bar{\eta}$ (see Table II) remains unexplained. Fortunately, fRG computations can be systematically improved through the parametrization of the effective action. In this way, high accuracy has been reached for non-disordered systems [60]. Refinements are probably feasible as well for the RFIM [61].

In conclusion, we have shown that the universality class of the RFIM is independent of the form of the implemented random-field distribution, in disagreement with the current opinion in the literature [33, 34, 37–40] and with the early predictions of mean-field theory [62]. To reach this conclusion, we had to identify and control the role of scaling corrections, the Achilles heel in the study of the RFIM (this problem was emphasized in the pioneering work of [35], but it was overlooked in subsequent investigations). On technical parts, we have developed a fluctuation-dissipation formalism that allowed us to compute correlation functions and to apply phenomenological renormalization. We have also adapted the approach of [63] to study the scaling of the energy (see Table III in the Appendix), checking that our data are compatible with modified hyperscaling [54] (a rather slippery problem [41]). Hence, several contradictions of previous works have been resolved in a consistent picture, paving the way to more sophisticated, experimentally relevant computations.

We were partly supported by MICINN, Spain, through research contracts No. FIS2009-12648-C03, FIS2012-35719-C02-01. Significant allocations of computing time were obtained in the clusters *Terminus* and *Memento* (BIFI). We are grateful to D. Yllanes and, especially, to L.A. Fernández for substantial help during several parts of this work. We also thank A. Pelissetto and G. Tarjus for useful correspondence.

[1] See T. Nattermann in [3].

[2] See D.P. Belanger in [3].

[3] *Spin Glasses and Random Fields*, A.P. Young (Ed.) (World Scientific, 1998).

[4] R.L.C. Vink, K. Binder, and H. Löwen, Phys. Rev. Lett. **97**, 230603 (2006).

[5] M.A. Annunziata and A. Pelissetto, Phys. Rev. E **86**, 041804 (2012).

- [6] E. Dagotto, *Science* **309**, 258 (2005).
- [7] J. Burgy, M. Mayr, V. Martín-Mayor, A. Moreo, and E. Dagotto, *Phys. Rev. Lett.* **87**, 277202 (2001).
- [8] J. Cardy and J.L. Jacobsen, *Phys. Rev. Lett.* **79**, 4063 (1997).
- [9] L.A. Fernández, A. Gordillo-Guerrero, V. Martín-Mayor, and J.J. Ruiz-Lorenzo, *Phys. Rev. Lett.* **100**, 057201 (2008).
- [10] L.A. Fernández, A. Gordillo-Guerrero, V. Martín-Mayor, and J. J. Ruiz-Lorenzo, *Phys. Rev. B* **86**, 184428 (2012).
- [11] J.P. Sethna, K. Dahmen, S. Kartha, J.A. Krumhansl, B.W. Roberts, and J.D. Shore, *Phys. Rev. Lett.* **70**, 3347 (1993).
- [12] O. Perković, K.A. Dahmen, and J.P. Sethna, *Phys. Rev. B* **59**, 6106 (1999).
- [13] D.M. Silevitch, G. Aeppli, and T.F. Rosenbaum, *Proc. Natl. Acad. Sci.* **107**, 2797 (2010).
- [14] Y. Imry and S.-K. Ma, *Phys. Rev. Lett.* **35**, 1399 (1975).
- [15] J. Villain, *Phys. Rev. Lett.* **52**, 1543 (1984).
- [16] A.J. Bray and M.A. Moore, *J. Phys. C: Solid. State Phys.* **18**, L927 (1985).
- [17] D.S. Fisher, *Phys. Rev. Lett.* **56**, 416 (1986).
- [18] A. Aharony, Y. Imry, and S.-K. Ma, *Phys. Rev. Lett.* **37**, 1364 (1976).
- [19] M. Gofman, J. Adler, A. Aharony, A.B. Harris, and M. Schwartz, *Phys. Rev. Lett.* **71**, 1569 (1993).
- [20] See e.g., D. Amit and V. Martín-Mayor, *Field Theory, the Renormalization Group and Critical Phenomena*, (World-Scientific Singapore, third edition, 2005).
- [21] A.P. Young, *J. Phys. A: Math. Gen.* **10**, L257 (1977).
- [22] G. Parisi and N. Surlas, *Phys. Rev. Lett.* **43**, 744 (1979).
- [23] J. Bricmont and A. Kupiainen, *Phys. Rev. Lett.* **59**, 1829 (1987).
- [24] G. Parisi, *Field Theory, Disorder and Simulations* (World Scientific, Singapore 1994).
- [25] G. Parisi and N. Surlas, *Phys. Rev. Lett.* **89**, 257204 (2002).
- [26] M. Tissier and G. Tarjus, *Phys. Rev. Lett.* **107**, 041601 (2011); *Phys. Rev. B* **85**, 104203 (2012).
- [27] Z. Slanič, D.P. Belanger, and J.A. Fernandez-Baca, *Phys. Rev. Lett.* **82**, 426 (1999).
- [28] F. Ye, M. Matsuda, S. Katano, H. Yoshizawa, D.P. Belanger, E.T. Seppälä, J.A. Fernandez-Baca, and M.J. Alava, *J. Magn. Magn. Mater.* **272**, 1298 (2004).
- [29] D.P. Belanger, A.R. King, V. Jaccarino, and J.L. Cardy, *Phys. Rev. B* **28**, 2522 (1983).
- [30] D.P. Belanger and Z. Slanič, *J. Magn. Magn. Mater.* **186**, 65 (1998).
- [31] V. Martín-Mayor, A. Pelisseto, and E. Vicari, *Phys. Rev. E* **66** 026112 (2002).
- [32] L.A. Fernández, V. Martín-Mayor, and D. Yllanes, *Phys. Rev. B* **84**, 100408 (2011).
- [33] N.G. Fytas, A. Malakis, and K. Eftaxias, *J. Stat. Mech.: Theory and Exp.* (2008) P03015.
- [34] B. Ahrens, J. Xiao, A.K. Hartmann, and H.G. Katzgraber, arXiv:1302.2480.
- [35] A.T. Ogielski, *Phys. Rev. Lett.* **57**, 1251 (1986).
- [36] J.-C. Anglès d'Auriac, Thesis, Grenoble (1986).
- [37] N. Surlas, *Comput. Phys. Commun.* **121**, 183 (1999).
- [38] J.-C. Anglès d'Auriac and N. Surlas, *Europhys. Lett.* **39**, 473 (1997).
- [39] M.R. Swift, A.J. Bray, A. Maritan, M. Cieplak, and J.R. Banavar, *Europhys. Lett.* **38**, 273 (1997).
- [40] A.K. Hartmann and U. Nowak, *Eur. Phys. J. B* **7**, 105 (1999).
- [41] A.K. Hartmann and A.P. Young, *Phys. Rev. B* **64**, 214419 (2001).
- [42] A.A. Middleton and D.S. Fisher, *Phys. Rev. B* **65**, 134411 (2002).
- [43] A.A. Middleton, *Phys. Rev. Lett.* **88**, 017202 (2002).
- [44] I. Dukovski and J. Machta, *Phys. Rev. B* **67**, 014413 (2003).
- [45] Y. Wu and J. Machta, *Phys. Rev. Lett.* **95**, 137208 (2005); *Phys. Rev. B* **74**, 064418 (2006).
- [46] H.G. Ballesteros, L.A. Fernández, V. Martín-Mayor, and A. Muñoz-Sudupe, *Phys. Lett. B* **378**, 207 (1996).
- [47] M.P. Nightingale, *Physica (Amsterdam)* **83A**, 561 (1976).
- [48] Severe ground-state degeneracy arises for discrete distributions, that needs to be taken into account, see S. Bastea and P.M. Duxbury, *Phys. Rev. E* **58**, 4261 (1998).
- [49] A.V. Goldberg and R.E. Tarjan, *J. Assoc. Comput. Mach.* **35**, 921 (1988).
- [50] For instance, in the Gaussian RFIM $G_{xy} = \overline{h_y \langle S_x \rangle} / \sigma^2$, see M. Schwartz and A. Soffer, *Phys. Rev. Lett.* **55**, 2499 (1985).
- [51] F. Cooper, B. Freedman, and D. Preston, *Nucl. Phys. B* **210**, 210 (1989).
- [52] G. Harris, *Nucl. Phys. B* **418**, 278 (1994).
- [53] H.G. Ballesteros, L.A. Fernández, V. Martín-Mayor, A. Muñoz-Sudupe, G. Parisi, and J.J. Ruiz-Lorenzo, *Phys. Rev. B* **58**, 2740 (1998); *Nucl. Phys. B* **512**, 681 (1998); *J. Phys. A* **30**, 8379 (1997); *Phys. Lett. B* **400**, 346 (1997).
- [54] N.G. Fytas and V. Martín-Mayor (in preparation).
- [55] Joint fits share the value of some fitting parameters such as the $L \rightarrow \infty$ extrapolation (which is the same for all random-field distributions), or the corrections-to-scaling exponent ω (which is common to all magnitudes).
- [56] Scaling corrections for the critical point are of order $L^{-(\omega+\frac{1}{\nu})}$, $L^{-(2\omega+\frac{1}{\nu})}$, etc. [20, 54].
- [57] The two-exponent scaling relation $\eta = (4 - D + 2\beta/\nu)/2$ yield $\eta = 0.5111(8)$, see [32]. However, this error is underestimated, as it does not consider scaling-corrections, nor the uncertainty in the critical value of \hat{m} .
- [58] T. Jolicoeur and F.J.-C. Le Guillou, *Phys. Rev. B* **56**, 10766 (1997).
- [59] C. Wetterich, *Phys. Lett.* **B301**, 90 (1993).
- [60] F. Benitez, J.-P. Blaizot, H. Chaté, B. Delamotte, R. Méndez-Galain, and N. Wschebor, *Phys. Rev. E* **85**, 026707 (2012).
- [61] G. Tarjus, private communication (2013).
- [62] A. Aharony, *Phys. Rev. B* **18**, 3318 (1978); *ibid.* **18**, 3328 (1978); D. Andelman, *ibid.* **27**, 3079 (1983).
- [63] C. Holm and W. Janke, *Phys. Rev. Lett.* **78**, 2265 (1997).

Appendix A: The critical exponent of the specific heat

In order to compute the specific-heat's critical exponent α , we consider the exchange part of the Hamiltonian (see main text for details):

$$E_{\text{exch}} = -J \sum_{\langle x,y \rangle} S_x S_y. \quad (\text{A1})$$

Finite-size scaling tell us that, at the critical point,

$$\overline{\langle E_{\text{exch}} \rangle} \sim A + BL^{\frac{\alpha-1}{\nu}} \quad (\text{A2})$$

where A and B are non-universal constants. Since $\alpha - 1$ is negative, Eq. (A2) is dominated by the non-divergent back ground A , forcing us to modify the standard phenomenological renormalization. We get rid of A by considering *three* lattices. At variance with the standard two-lattices phenomenological renormalization, statistical errors are significantly amplified by the reweighting extrapolation. Hence, we have preferred to carry out an independent set of simulations for parameters corresponding to the crossing points identified in the main manuscript and listed on Table IV. Our results for $(\alpha - 1)/\nu$ are given in Table III. Details will be provided elsewhere (see N.G. Fytas and V. Martín-Mayor, manuscript in preparation).

TABLE III: Effective critical exponent ratio $(\alpha - 1)/\nu$ using a three-lattice size variant $(L_1, L_2, L_3) = (L, 2L, 4L)$ of the quotients method.

Distr.	(L_1, L_2, L_3)	$(\alpha - 1)/\nu$
G	(12, 24, 48)	-0.758(11)
	(16, 32, 64)	-0.793(17)
	(24, 48, 96)	-0.860(30)
	(32, 64, 128)	-0.881(75)
dG ^($\sigma=1$)	(16, 32, 64)	0.954(66)
	(24, 48, 96)	-0.036(23)
	(32, 64, 128)	-0.309(23)
dG ^($\sigma=2$)	(12, 24, 48)	-0.735(16)
	(16, 32, 64)	-0.766(16)
	(24, 48, 96)	-0.882(60)
	(32, 64, 128)	-0.867(56)
P	(12, 24, 48)	-1.120(6)
	(16, 32, 64)	-1.089(10)
	(24, 48, 96)	-1.071(42)
	(32, 64, 128)	-0.970(37)

Appendix B: Raw results from the quotients method

The effective, lattice-size dependent estimations of critical points, critical exponents, and dimensionless universal constants are reported on Table IV. See main text for definitions and details on our phenomenological renormalization method.

TABLE IV: Crossing points, universal ratios, and effective critical exponents of the $D = 3$ RFIM as given from the application of the quotients method for all four types of distributions considered.

Distr.	(L_1, L_2)	crossings	U_4	ξ/L	ν	$\xi^{(\text{dis})}/L$	$\nu^{(\text{dis})}$	η	$\bar{\eta}$	$2\eta - \bar{\eta}$
G	(16, 32)	2.2779(3)	1.0030(1)	1.937(3)	1.48(3)	7.57(2)	1.36(3)	0.5168(6)	1.0298(2)	0.0038(11)
	(24, 48)	2.2758(2)	1.0028(1)	1.966(3)	1.45(3)	7.75(2)	1.39(4)	0.5155(5)	1.0289(2)	0.0022(11)
	(32, 64)	2.2745(1)	1.00261(4)	1.989(3)	1.36(4)	7.88(2)	1.43(5)	0.5150(5)	1.0280(1)	0.0019(10)
	(48, 96)	2.2734(1)	1.00263(9)	2.019(3)	1.43(6)	8.04(2)	1.45(6)	0.5154(5)	1.0275(2)	0.0033(9)
	(64, 128)	2.2731(1)	1.0025(1)	2.028(3)	1.38(9)	8.07(2)	1.35(9)	0.5142(5)	1.0271(3)	0.0014(10)
	(96, 192)	2.2727(1)	1.00243(5)	2.042(4)	1.38(11)	8.15(2)	1.34(11)	0.5144(5)	1.0268(1)	0.0021(11)
dG $^{(\sigma=1)}$	(16, 32)	1.9311(4)	1.00030(4)	4.340(17)	3.04(14)	21.21(12)	1.49(3)	0.5035(7)	1.0055(1)	0.0016(15)
	(24, 48)	1.9751(2)	1.00094(1)	2.868(7)	2.26(9)	12.66(5)	1.42(3)	0.5083(7)	1.0131(1)	0.0034(14)
	(32, 64)	1.9874(1)	1.00137(2)	2.494(4)	1.87(8)	10.58(3)	1.46(4)	0.5093(7)	1.0176(1)	0.0010(13)
	(48, 96)	1.9947(1)	1.00181(2)	2.251(3)	1.56(9)	9.27(2)	1.38(5)	0.5121(7)	1.0217(1)	0.0026(14)
	(64, 128)	1.9968(1)	1.00205(1)	2.170(3)	1.67(12)	8.83(2)	1.39(5)	0.5125(8)	1.0235(1)	0.0015(17)
dG $^{(\sigma=2)}$	(16, 32)	1.0741(5)	1.00275(4)	1.962(4)	1.48(5)	7.71(2)	1.36(4)	0.5154(6)	1.0287(1)	0.0020(12)
	(24, 48)	1.0722(4)	1.00265(4)	1.976(3)	1.50(6)	7.80(2)	1.44(6)	0.5151(7)	1.0282(2)	0.0020(13)
	(32, 64)	1.0708(3)	1.0026(1)	1.989(3)	1.41(8)	7.87(2)	1.48(9)	0.5142(7)	1.0281(2)	0.0004(13)
	(48, 96)	1.0683(3)	1.00250(5)	2.017(4)	1.36(10)	8.03(2)	1.36(9)	0.5148(7)	1.0273(2)	0.0024(14)
	(64, 128)	1.0671(2)	1.00244(2)	2.038(3)	1.31(11)	8.13(2)	1.31(11)	0.5154(6)	1.0267(1)	0.0041(13)
P	(16, 32)	1.7734(2)	1.00363(2)	1.794(3)	1.20(2)	6.71(2)	1.09(2)	0.5183(9)	1.0373(1)	-0.0006(19)
	(24, 48)	1.7659(2)	1.00310(5)	1.894(4)	1.26(3)	7.29(2)	1.26(3)	0.5168(8)	1.0325(2)	0.0011(17)
	(32, 64)	1.7625(2)	1.00278(2)	1.955(4)	1.30(4)	7.64(2)	1.34(4)	0.5153(8)	1.0301(1)	0.0005(17)
	(48, 96)	1.7605(1)	1.00259(4)	2.005(3)	1.37(7)	7.92(2)	1.41(6)	0.5143(9)	1.0282(1)	0.0004(18)
	(64, 128)	1.7596(1)	1.00248(3)	2.030(3)	1.33(7)	8.06(2)	1.35(7)	0.5148(8)	1.0273(1)	0.0024(16)
	(96, 192)	1.7589(1)	1.00247(9)	2.060(5)	1.43(13)	8.22(3)	1.48(13)	0.5146(8)	1.0266(1)	0.0026(17)